# Anomalous Hall effect in conical helimagnetic crystals

Andrei Zadorozhnyi and Yuri Dahnovsky 6\*

Department of Physics and Astronomy/3905, 1000 E. University Avenue, University of Wyoming, Laramie, Wyoming 82071, USA



(Received 26 September 2022; revised 1 December 2022; accepted 23 December 2022; published 12 January 2023)

Spin-spiral texture can substantially change charge transport properties in helimagnets. We find the anomalous Hall effect (AHE) exhibiting the dramatic behavior with respect to chemical potential  $\mu$  in conical magnetic structures. The direct conductivity demonstrates kinks, and the anomalous Hall current exhibits minima and maxima changing the sign. We analytically derive the expression for energy bands and eigenstates in the most general case. Because of the conical potential, the energy bands are split into two nonparabolic bands where the lower band can have one- or two-minima shapes in the  $k_z$  direction ( $\hat{z}$  is a direction of the spiral axis). We prove that the origin of the anomalous Hall effect is not topological and is due to the interplay between the asymmetry of energy bands in the x and z directions and spin restrictions in the phase space due to the conical potential. We also investigate the dependence of transport properties on cone half- angle  $\theta$ , and find that the effects are most pronounced at  $\theta = \pi/2$  (a helical state). Electric current is calculated using the Boltzmann equation where the relaxation is caused by electron-acoustic phonon interaction. The transition probability is found to be a 2 × 2 matrix with nonvanishing off-diagonal elements indicating the strong interband transitions. The origin of interband transitions is because of the nature of the conical potential where conduction electron spins interact with localized magnetic moments. To verify the proposed theory, we calculate the temperature dependence of resistivity for MnSi crystals and find the discontinuity at the phase transition between conical and paramagnetic phases. The calculations are in the excellent agreement with the experimental data. In addition, we predict the discontinuity behavior for the anomalous Hall resistivity at the phase transition where the resistivity exhibits the abrupt change at  $T = T_C$ , (a) to zero if the relativistic effects for the conduction electrons are small or (b) to a nonzero value if Rashba/Dresselhaus effects are taken into account.

## DOI: 10.1103/PhysRevB.107.035202

## I. INTRODUCTION

Helimagnetism can be originated from both relativistic corrections [1–4] and exchange interaction with spin frustrations [5]. A conical phase can be one of phases in a phase diagram [6,7]. The conical phases were experimentally observed in  $U_3P_4$  [8],  $\gamma$  – Fe [9], and MnP [10] crystals. Because of the interaction between a conduction electron spin and magnetic moments of the conical magnetic structure, we expect that charge transport properties will have unusual behaviors, which can be theoretically understood from the calculations employing the Boltzmann equation for a nonequilibrium distribution function. The Boltzmann equation approach has the advantage because it allows for the consideration of realistic electron scattering mechanisms such as electron-phonon or electron-impurity scattering. For electron scattering in pure crystals, we choose the electron-phonon scattering as the main electron scattering mechanism. Along with electronic structure and transport in conical spin spirals, we also study the Berry curvature to understand whether such materials are topological. The chirality is also investigated.

To describe the transport properties in 3D conical magnetic materials, we consider the following Hamiltonian [9]:

$$\hat{H}_{0} = \hat{H}_{\text{crys}} + \hat{H}_{\text{con}} = \frac{\hbar^{2} k^{2}}{2m} - JS_{0}\hat{\boldsymbol{\sigma}} \cdot \boldsymbol{n}(\boldsymbol{r})$$

$$= \frac{\hbar^{2} k^{2}}{2m} - JS_{\parallel}(\sigma_{x} \cos(\varkappa z) + \sigma_{y} \sin(\varkappa z)) - JS_{z}\sigma_{z},$$
(1)

where J is an exchange integral between the conduction electrons and localized magnetic moments  $S_0$ . Here  $\sigma$  is the vector of the three Pauli matrices. The spiral period of the localized spin rotation about the z axis is  $2\pi/\varkappa$ . Spin-orbit coupling should be in general considered for both conduction and localized electrons. Nevertheless, for the conduction electrons such effects can be weak because the Rashba/Dresselhaus constants can be numerically small. Moreover, there are materials that exhibit spin-spiral properties without spin-orbit coupling, for example, FeP [5]. In the latter case the origin of the helical structure is due to spin frustration in Heisenberg spin-spin interaction originating from the electron exchange mechanism. However, we should note that the Rashba/Dresselhaus interaction can dramatically alter the behavior of anomalous Hall conductivity in other materials, for example, in a skyrmion phase [11]. In this paper we do not consider spin-orbit coupling for conduction electrons, even if it is responsible for the spiral spin structures. Therefore, all the effects we consider here arise from the exchange interaction between the

<sup>\*</sup>yurid@uwyo.edu

spin spiral and the conduction electron. This approach was previously employed for electrons in the presence of helical spin-structures [9,12,13] and skyrmions [14,15].

We organize this paper in the following way: Hamiltonian (1) is diagonalized in Sec. II where band structures and wavefunctions are found in the most general form. The Boltzmann equation approach and electron-phonon transition rate calculations are discussed in Sec. III. The transport properties including the anomalous Hall electroconductivity are calculated in Sec. IV. The comparison between the theoretical predictions and experimental data for MnSi crystals is discussed in Sec. V. The Berry curvature and chirality are calculated in Sec. VI.

### II. ELECTRONIC STRUCTURE

In this section we find eigenstates and eigenvalues of Hamiltonian (1). To do this, we employ the Wannier theorem [16],

$$\left[\varepsilon_0(-i\nabla) + \sum_{s'} V_{ss'}(\mathbf{r})\right] \Psi_{\mathbf{k}}^s = \varepsilon \Psi_{\mathbf{k}}^s. \tag{2}$$

In this equation  $\varepsilon_0$  is the energy band where the conical potential is not considered.  $V_{ss'}(\mathbf{r})$  is a conical potential. To diagonalize the Hamiltonian, we present the wavefunction as

follows:

$$\Psi_k^s = \psi_{0k}(\mathbf{r})\Psi_{zk}^s(z),\tag{3}$$

where  $\psi_{0k}$  is an unperturbed wavefunction satisfying the following equation:

$$\varepsilon_0(-i\nabla)\psi_{0k}(\mathbf{r}) = \varepsilon_0(\mathbf{k})\psi_{0k}(\mathbf{r}). \tag{4}$$

Then, we substitute wavefunction (3) into Wannier Equation (2) resulting in the following expression for the total wavefunctions,

$$\begin{pmatrix} \Psi_{k,\varkappa}^{\uparrow(\nu)}(r) \\ \Psi_{k,\varkappa}^{\downarrow(\nu)}(r) \end{pmatrix} = \begin{pmatrix} a_{\nu}(k,\varkappa)e^{-i\frac{\varkappa}{2}z} \\ b_{\nu}(k,\varkappa)e^{+i\frac{\varkappa}{2}z} \end{pmatrix} \psi_{0k}(r).$$
 (5)

Here,  $a_{\nu}$  and  $b_{\nu}$  are coefficients independent of the coordinates. Index  $\nu = 1, 2$  designates a band number. Then, we insert wavefunction (5) back into Eq. (2) resulting in the two linear equations for the coefficients  $a_{\nu}$  and  $b_{\nu}$ ,

$$-a_{\nu}JS_{z} - b_{\nu}JS_{\parallel} + a_{\nu}\varepsilon_{0}\left(k_{x}, k_{y}, k_{z} - \frac{\varkappa}{2}\right) = a_{\nu}\varepsilon_{\nu},$$

$$b_{\nu}JS_{z} - a_{\nu}JS_{\parallel} + b_{\nu}\varepsilon_{0}\left(k_{x}, k_{y}, k_{z} + \frac{\varkappa}{2}\right) = b_{\nu}\varepsilon_{\nu}. \quad (6)$$

Here  $\varepsilon_0(\mathbf{k})$  is taken in the most general form. Using Eq. (6), we find the expression for  $\varepsilon_{1,2}$ ,

$$\varepsilon_{1,2} = \frac{\varepsilon_0(\mathbf{k} + \mathbf{e}_z \frac{\varkappa}{2}) + \varepsilon_0(\mathbf{k} - \mathbf{e}_z \frac{\varkappa}{2})}{2} \pm \sqrt{J^2 S_{\parallel}^2 + \left[\frac{\varepsilon_0(\mathbf{k} + \mathbf{e}_z \frac{\varkappa}{2}) - \varepsilon_0(\mathbf{k} - \mathbf{e}_z \frac{\varkappa}{2})}{2} + J S_z\right]^2} \\
= \frac{\varepsilon_0(\mathbf{k} + \mathbf{e}_z \frac{\varkappa}{2}) + \varepsilon_0(\mathbf{k} - \mathbf{e}_z \frac{\varkappa}{2})}{2} \pm \sqrt{J^2 S_{\parallel}^2 + [D + J S_z]^2}, \tag{7}$$

where  $D = [\varepsilon_0(\mathbf{k} + \mathbf{e}_z \frac{\varkappa}{2}) - \varepsilon_0(\mathbf{k} - \mathbf{e}_z \frac{\varkappa}{2})]/2$ . From the normalization conditions and Eqs. (6) and (7), we determine the coefficients  $a_v$  and  $b_v$ ,

$$a_{1} = b_{2} = \frac{1}{\sqrt{2}} \frac{\sqrt{\sqrt{J^{2}S_{\parallel}^{2} + (D + JS_{z})^{2} + (D + JS_{z})}}}{(J^{2}S_{\parallel}^{2} + (D + JS_{z})^{2})^{1/4}},$$

$$a_{2} = -b_{1} = -\frac{1}{\sqrt{2}} \frac{\sqrt{\sqrt{J^{2}S_{\parallel}^{2} + (D + JS_{z})^{2}} - (D + JS_{z})}}{(J^{2}S_{\parallel}^{2} + (D + JS_{z})^{2})^{1/4}}.$$
(8)

For further calculations we consider a parabolic form for  $\varepsilon_0(\mathbf{k})$ .  $\varepsilon_{1,2}(\mathbf{k})$  are presented Fig. 1. As shown in Fig. 1(a),  $\varepsilon_{1,2}(\mathbf{k})$  are symmetric paraboloids where  $JS_{\parallel}=0$  (a pure ferromagnetic state). The helical state with the single minimum in  $\varepsilon_1(\mathbf{k})$  (the  $S_z=0$ ,  $\hbar^2\varkappa^2/2m<2JS_{\parallel}$  case) is depicted in Fig. 1(b). As shown in Fig. 1(c),  $\varepsilon_1(\mathbf{k})$  has two symmetric minima in the  $k_z$  direction for a helical state  $(\hbar^2\varkappa^2/2m>2JS_{\parallel})$ . Case (d) corresponds to the conical state  $(S_z\neq 0, S_{\parallel}\neq 0)$  where the bands are asymmetric in the  $k_z$  direction. The two-minima shape of  $\varepsilon_1(\mathbf{k})$  is a saddle rather than a Mexican-hat shape discussed in Ref. [11] for the Rashba effect. Indeed, in x and y directions  $\varepsilon_1(\mathbf{k})$  are still parabolas.

## III. TRANSPORT IN CONICAL SPIN-SPIRALS

### A. Boltzmann equation

For the transport calculations we employ the Boltzmann equation with the relaxation rate due to electron-phonon interaction.

$$\frac{\partial f_0}{\partial \varepsilon} e \boldsymbol{E} \cdot \boldsymbol{v}^{\nu} = \sum_{\nu'} \sum_{\boldsymbol{k'}} \left( W_{\boldsymbol{k}\boldsymbol{k'}}^{\nu\nu'} f_1^{\nu'}(\boldsymbol{k'}) - W_{\boldsymbol{k'}\boldsymbol{k}}^{\nu'\nu} f_1^{\nu}(\boldsymbol{k}) \right). \tag{9}$$

 $f_0$  is the equilibrium Fermi distribution function,  $f_1$  is the nonequilibrium part of the total distribution function, E is an applied electric field, v is an electron velocity. The transition rates  $W_{k\nu'}^{\nu\nu'}$  are defined as follows:

$$W_{\mathbf{k}\mathbf{k}'}^{\nu\nu'} = (2\pi/\hbar)|\langle \mathbf{k}', \nu', N_{\mathbf{q}j}'|\Delta V|\mathbf{k}, \nu, N_{\mathbf{q}j}\rangle|^2 \delta(\varepsilon_{\nu}(\mathbf{k}) - \varepsilon_{\nu'}(\mathbf{k}')).$$
(10)

In this equation  $\Delta V$  is the electron-phonon interaction potential.  $N_{qj}$  is the population number of phonons with the wavevector  $\mathbf{q}$  and the branch j determined from the Bose distribution function.

$$N_{qj} = \frac{1}{e^{\frac{\epsilon_{ph}}{k_B T}} - 1}. (11)$$

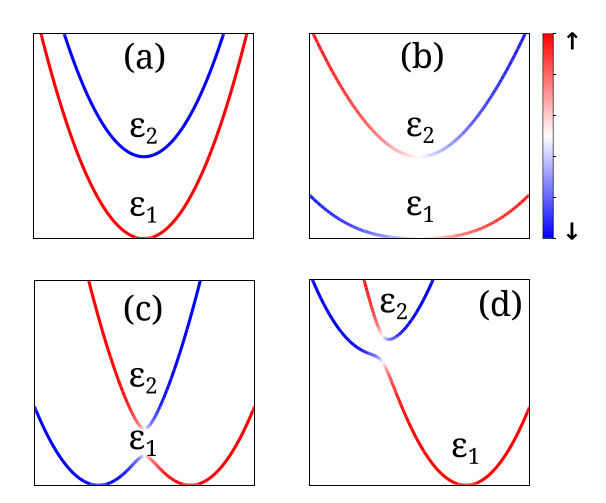


FIG. 1. Band structures for  $\varepsilon_1$  and  $\varepsilon_2$  in for four different cases. (a) The ferromagnetic phase  $(S_{\parallel}=0,\ S_z\neq 0)$  where  $\varepsilon_{1,2}(k)$  are paraboloids; (b) a helical state  $(S_z=0)$  where  $\varepsilon_1(k)$  has one non-parabolic minimum  $(\hbar^2\varkappa^2/2m < 2JS_{\parallel})$ ; (c) a helical state where  $\varepsilon_1(k)$  has two symmetric minima  $(\hbar^2\varkappa^2/2m > 2JS_{\parallel})$ ; and (d) conical phase  $(S_z\neq 0,\ S_{\parallel}\neq 0)$  where the bands are asymmetric. The blue color corresponds to the spin- $\downarrow$  projection and the red color represents the spin- $\uparrow$  projection. The mixture of the spin-up and spin-down states is shown in the middle region.

Index  $\nu$  denotes an energy band number ( $\nu = 1, 2$ ). As soon as the transition rates are found and the Boltzmann equation is solved, we can determine the electric current density

$$j_i^{\nu} = e \frac{1}{(2\pi)^3} \int f_1^{\nu} v_i^{\nu} d^3 k, \qquad (12)$$

where  $v_i^{\nu}$  is a velocity projection (i=x,y,z) determined as  $v_i^{\nu}=\partial \varepsilon^{\nu}(\pmb{k})/\hbar \partial k_i$ . To solve the Boltzmann Equation (9), we have written the

To solve the Boltzmann Equation (9), we have written the original codes where the relaxation rates are considered within the first Born approximation. We have used nonparabolic  $\varepsilon_1(k)$  and  $\varepsilon_2(k)$  for the solution of the Boltzmann equation. The numerical codes include the calculation of constant energy surface, which contains multiple subsurfaces. For each  $(\nu, k)$  and  $(\nu', k')$  at the energy surface, the transition rates have been found and substituted into the integral Boltzmann equation, which has been numerically solved for  $f_1$  in the piecewise constant approximation and then is inserted into the expression for the current [see Eq. (18)].

## **B.** Transition rates

Bearing in mind that the system is a pure crystal with no impurities, the electron scattering results only from the electron-phonon interaction. The phonon system includes acoustic and optical phonons. We consider only acoustic phonons for the electron-phonon interaction. Indeed, in MnSi the optical phonon with the lowest frequency is about hv = 22 meV = 225 K. The conical state exists only below 29 K [17,18]. Since the optical phonon contribution is about  $\exp(-hv/kT) \sim 10^{-3}$ , it can be safely disregarded. The electron-phonon interaction is considered in the following form:

$$\hat{V}_{e-nh} \approx -\nabla (\hat{H}_{crvs} + \hat{H}_{con}) \cdot \boldsymbol{u}. \tag{13}$$

 $\hat{H}_{crys}$  and  $\hat{H}_{con}$  are defined in Eq. (1). The atom displacement u can be expressed in terms of normal phonon coordinates. The matrix element in Eq. (10) is determined for electron and phonon wavefunctions separately. If we consider the phonons in equilibrium, then the contribution for the absorption and emission of a phonon with a wave vector q by the electron is given by the following expression [16]:

$$L = \langle N_{qj} - 1 | a_{qj} | N_{qj} \rangle = \sqrt{\frac{\hbar N_{qj}}{2\omega_{qj}}},$$

$$L^{+} = \langle N_{qj} + 1 | a_{qj}^{+} | N_{qj} \rangle = \sqrt{\frac{\hbar (N_{qj} + 1)}{2\omega_{qj}}}.$$
(14)

The averaging over the electron wavefunctions is more complicated. Indeed, the electron wavefunctions have two components (5) resulting in a  $2 \times 2$  matrix for the transition probabilities. We omit the derivation of the transition rate because the procedure of the calculation of the matrix elements is similar to that of presented in Refs. [16,19]. The final expression for the transition probabilities is given by the equation

$$W_{kk'}^{\nu\nu'} = \frac{2\pi}{\hbar} \frac{1}{NM} \frac{\hbar N_{qj}}{2\omega_{q}} |K_{\nu\nu'}^{+}|^{2} \delta(\varepsilon_{\nu}(\mathbf{k}) - \varepsilon_{\nu'}(\mathbf{k}')) \delta(\mathbf{k}' - \mathbf{k} - \mathbf{q})$$

$$+ \frac{2\pi}{\hbar} \frac{1}{NM} \frac{\hbar (N_{-qj} + 1)}{2\omega_{-q}} |K_{\nu\nu'}^{-}|^{2} \delta(\varepsilon_{\nu}(\mathbf{k})$$

$$- \varepsilon_{\nu'}(\mathbf{k}')) \delta(\mathbf{k}' - \mathbf{k} + \mathbf{q}), \tag{15}$$

where  $K_{uv'}^{\pm}$  are defined by the following equations:

$$K_{\nu\nu'}^{\pm} = \mp \sum_{s} i \frac{\hbar^{2}}{m} (\mathbf{k} - \mathbf{k}') \cdot \int (\nabla u_{sk}^{\nu}) (\mathbf{e}_{qj} \cdot \nabla u_{sk'}^{\nu'*}) d\tau_{0}$$

$$\mp \sum_{s} \left[ \varepsilon^{\nu}(\mathbf{k}) - \varepsilon^{\nu'}(\mathbf{k}') - \left( \frac{\hbar^{2} k^{2}}{2m} - \frac{\hbar^{2} k'^{2}}{2m} \right) \right]$$

$$\times \int u_{sk}^{\nu} (\mathbf{e}_{qj} \cdot \nabla u_{sk'}^{\nu'*}) d\tau_{0}. \tag{16}$$

Substituting the wavefunctions from Eq. (5) into Eq. (16) and assuming that the period of the conical spiral is much greater than the lattice constant a ( $\varkappa a \ll 1$ ), and keeping the terms of the order of  $a^{-2}$ , we obtain the final expression for  $K_{uu'}^{\pm}$ ,

$$K_{\nu\nu'}^{\pm} = \pm i \frac{\hbar^2}{2ma^2} \frac{2}{3} (\mathbf{q} \cdot \mathbf{e}_{\mathbf{q}j}) (a_{\nu}(\mathbf{k}) a_{\nu'}(\mathbf{k}') + b_{\nu}(\mathbf{k}) b_{\nu'}(\mathbf{k}')), \tag{17}$$

where  $a_{\nu}$  and  $b_{\nu}$  are described in Eq. (8). From Eq. (17) there is a probability of the electron to scatter from  $\nu$  to  $\nu' \neq \nu$ , i.e., interband transitions are allowed.

### IV. RESULTS AND DISCUSSIONS

In this paper we perform the calculations with the parameters chosen for a MnSi pure crystal. The acoustic phonons are considered in the Debye approximation with  $\omega_D = v_0(6\pi^2/\Omega_0)$ ,  $v_0$  is a velocity of sound, and  $\Omega_0$  is a unit-cell volume. We have chosen MnSi for numerical estimation where  $v_s = 740 \text{ m/s}$  [20] and  $\Omega_0 = 0.092 \text{ nm}^3$ . According to

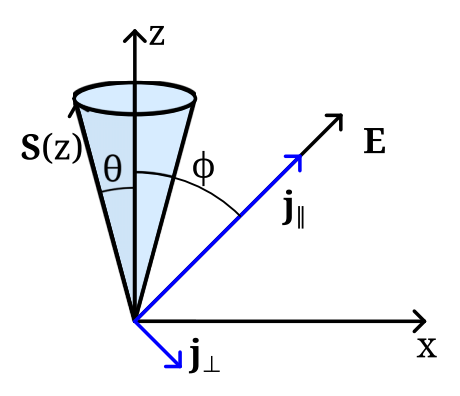


FIG. 2. Geometry of the spin-spiral direction and the electric field E direction. The current has two components,  $j_{\parallel}$  along the electric field and  $j_{\perp}$  perpendicular to the electric field (anomalous Hall current). The angle between the spiral axis and the electric field is  $\phi$ , and a cone half-angle is  $2\theta$ .

Ref. [16], the elastic scattering is a good approximation for the numerical calculations where the transition rate matrix elements are given by Eq. (15).

If there is a nonvanishing angle  $\phi$  between the spiral axis and the electric field, there are two electric current components,  $j_{\parallel}$  along the electric field and  $j_{\perp}$  perpendicular to the electric field (anomalous Hall current) as shown in Fig. 2. The expression for the current in this case was found if Ref. [11],

$$j_{\parallel}^{s} = j_{0\parallel}^{s} + j_{2}^{s} \cos(2\phi), \quad j_{\perp}^{s} = j_{0\perp}^{s} + j_{2}^{s} \sin(2\phi).$$
 (18)

Because of the absence of the specific direction (the cylindrical symmetry in x, y plane) for the anomalous Hall component  $j_{0\perp}$ , the angle-independent component in the second equation in (18),  $j_{0\perp}^s$ , vanishes.

We calculate the dependence of electroconductivity in parallel and perpendicular directions with respect to chemical potential  $\mu$ . The chemical potential (or  $\varepsilon_F$ , Fermi energy) can be varied by the gate voltage in a proper electronic device. For the calculations we have chosen the parameters close to those of MnSi single crystals. In Figs. 3, and 4 7, 9 we

consider different cone half-angles ( $\theta=0,\pi/16,\pi/4,\pi/2$ ). The case where the cone half-angle  $\theta=0$  corresponds to a pure ferromagnetic state, and  $\theta=\pi/2$  represents a helical spin-spiral phase.

The direct and anomalous Hall components in a pure ferromagnetic state are presented in Fig. 3. This case corresponds to the band arrangement shown in Fig. 1(a). In Fig. 3(a), the direct conductivities are growing functions, and the anomalous Hall conductivities due to the spin spiral in Fig. 3(b) are zero because of the spherical symmetry of  $\varepsilon(k)$ .

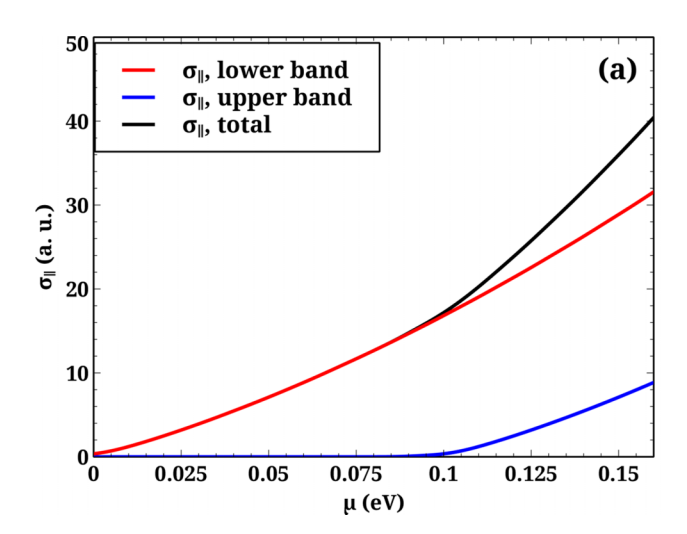
If the cone half-angle is  $\theta = \pi/16$ , we find the unusual behavior in both direct and anomalous Hall components of the electric conductivity. This case corresponds to the band structures shown in Fig. 1(d). Indeed, the two kinks in red and black curves are depicted in Fig. 4(a). The first kink takes place at  $\mu = 0.095 \,\text{eV}$ , and can be explained using Fig. 1(d). Indeed, as soon as  $\mu$  reaches the region of spin-down electrons shown in blue color in  $\varepsilon_1$ , the phase volume increases and therefore, the electric current [see Eq. (18)] grows. The second kink occurs at  $\mu$  approaching the upper band, which begins to contribute to scattering decreasing the current value. The insertion in Fig. 4(a) demonstrates the dramatic derivative change in the vicinity of the kinks' regions. Contrary to the ferromagnetic case [see Fig. 3(b)], there is the unusual behavior in the anomalous Hall electroconductivity. As shown in Fig. 4(b), the anomalous Hall component exhibits the two peaks. To explain such an behavior, we use the explanation based on a simplified model where W is k independent. According to Ref. [16], the transition probability per unit time can be calculated using the following formula:

$$\frac{1}{\tau} = \int W(\theta)(1 - \cos \theta) d\Omega. \tag{19}$$

If we assume  $W(\theta) = const$  (angle independent), we can easily evaluate  $1/\tau$ , where

$$\frac{1}{\tau} = 2\pi W \left[ \frac{3}{4} + \cos(\theta_0) + \frac{1}{4} \cos(2\theta_0) \right]. \tag{20}$$

For the derivation we notice that the integration takes place only in a restricted phase space for single spin shown in Fig. 5.



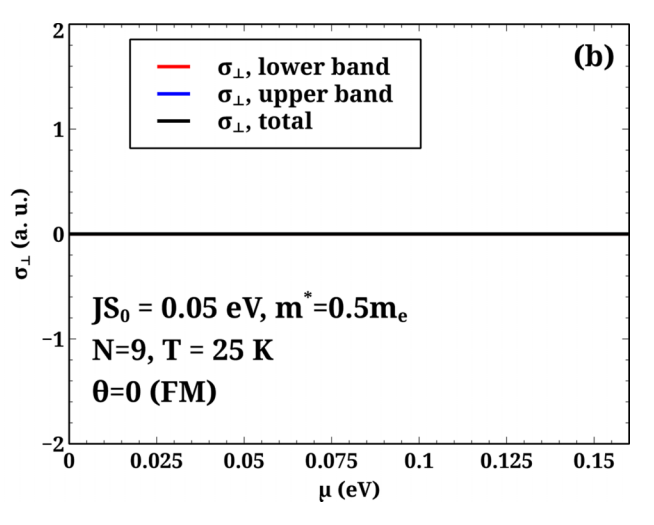
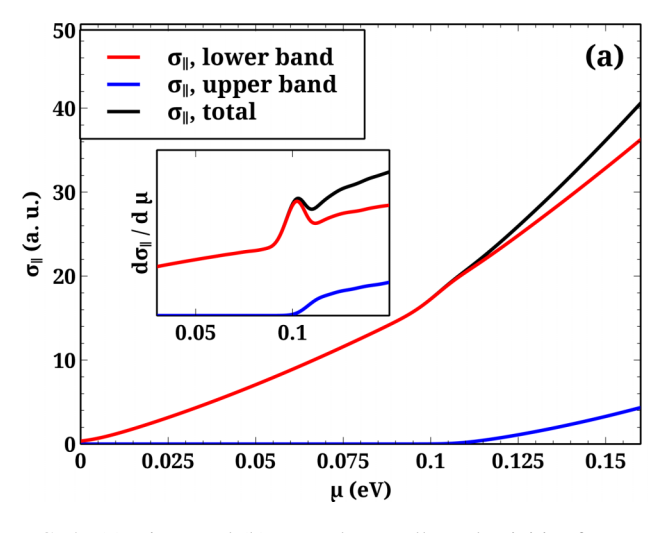


FIG. 3. (a) Direct and (b) anomalous Hall conductivities for the ferromagnetic case. The blue curve represents the conductivity for the upper band, and the red curve is for the lower band. The black line corresponds to the total electroconductivity.



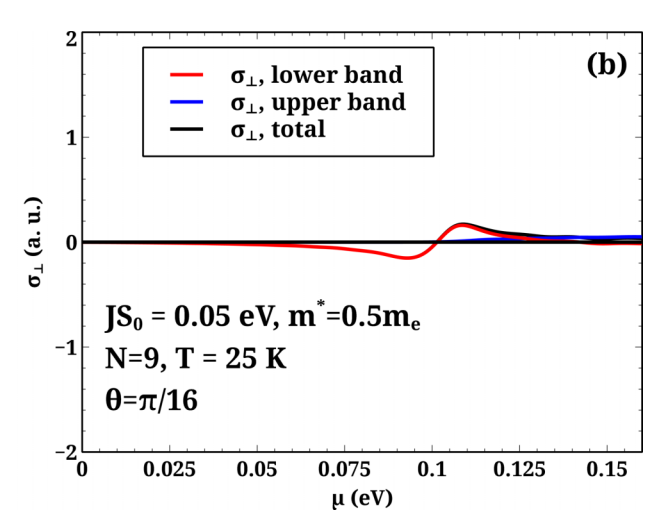


FIG. 4. (a) Direct and (b) anomalous Hall conductivities for  $\theta = \pi/16$ . The blue curves represent the conductivities for the upper band, and the red curves are for the lower band. The black lines describe the total electroconductivity. In the insertion the derivative of the direct component of the conductivity over chemical potential is presented

 $\theta_0 = \theta_0^{\uparrow,\downarrow}$  are defined in Fig. 5. The current density can be calculated according to Ref. [16], where  $\tau$  is found in Eq. (20),

$$\mathbf{j} = -\frac{e^2}{4\pi^3} \int \tau(\mathbf{k}) \frac{\partial f_0}{\partial \varepsilon} \mathbf{v} (\mathbf{v} \cdot \mathbf{E}) d^3 k 
= \frac{2m^*}{\hbar^2} \frac{e^2}{4\pi^2} \tau k_F^2 v_F^2 \frac{1}{12} \begin{pmatrix} E_x(9\cos(\theta_0) - \cos(3\theta_0) + 8) \\ E_y(9\cos(\theta_0) - \cos(3\theta_0) + 8) \\ E_z(6\cos(\theta_0) + 2\cos(3\theta_0) + 8) \end{pmatrix}.$$
(21)

The anomalous Hall current can be determined as follows:

$$j_{\perp} = j \sin \alpha = \left[ j \times \frac{E}{|E|} \right]_{y} = E_{x} E_{z} (\sigma_{zz} - \sigma_{xx}) / |E|, \quad (22)$$

where  $\alpha$  is an angle between the current and the electric field,

$$\sigma_{zz} - \sigma_{xx} = \frac{2m^*}{\hbar^2} \frac{e^2}{4\pi^2} \tau k_F^2 v_F^2 \frac{1}{12} (3\cos(3\theta_0) - 3\cos\theta_0),$$

$$\underset{\theta_0 \to 0}{\approx} -\frac{2m^*}{\hbar^2} \frac{e^2}{4\pi^2} \tau k_F^2 v_F^2 \frac{1}{12} \times 24\theta_0^2 < 0. \quad (23)$$

As demonstrated in Eq. (23), the current is negative for small  $\theta_0^{\uparrow,\downarrow}$  ( $\theta_0^{\uparrow,\downarrow}$  is defined in Fig. 5). This means that the

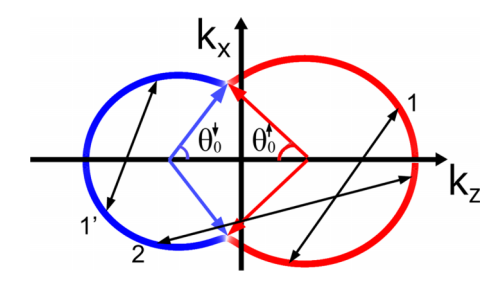


FIG. 5. Energy surface cross section in  $k_x$ ,  $k_z$  plane for the lower band. The red and blue colors correspond to the spin-up and spin-down states, respectively. Two-sided arrows 1 and 1' correspond to allowed transitions with the same spin  $\uparrow$  and  $\downarrow$  respectively. Line 2 demonstrates the spin-forbidden transition.

current tends to lean towards the x axis, as shown in Fig. 4 (the negative value of  $\sigma_{\perp}$ ). Then, according to this figure, the current goes up because the transition probability W is asymmetric with respect to scattering in the x and z directions. Indeed, in the  $k_x$  direction the transition rates are stronger because of the larger phase volume and weaker in the  $k_z$  direction because of the restricted scattering rate in this direction. Thus, we conclude that the current in the x direction is lower than in the x one. From this consideration, it follows that the current leans towards x axis, and therefore |x| = |x| decreases. By adding the upper band there are more carriers and therefore, the current increases in the x-direction. It would increase further up unless the bands become spherical. To explain the maximum in the positive region we have to introduce the two parabolic energy bands,

$$\varepsilon_{1,2}^{na} \approx \frac{\hbar^2}{2m} (k_x^2 + k_y^2 + (k_z \pm \varkappa/2)^2) \pm JS_z.$$
 (24)

 $\varepsilon_{1,2}^{na}$  are shown in Fig. 6. In this case each energy band has the spherical symmetry and therefore, the anomalous Hall electroconductivity vanishes.

We also study the cone half-angle  $\theta = \pi/4$  (see Fig. 7). The dependencies for both  $\sigma_{\parallel}$  and  $\sigma_{\perp}$  are similar to the previous case,  $\theta = \pi/16$ . However, the effects are more

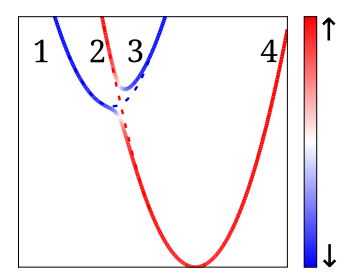


FIG. 6. Energy bands. A spin projection is conserved for each band.

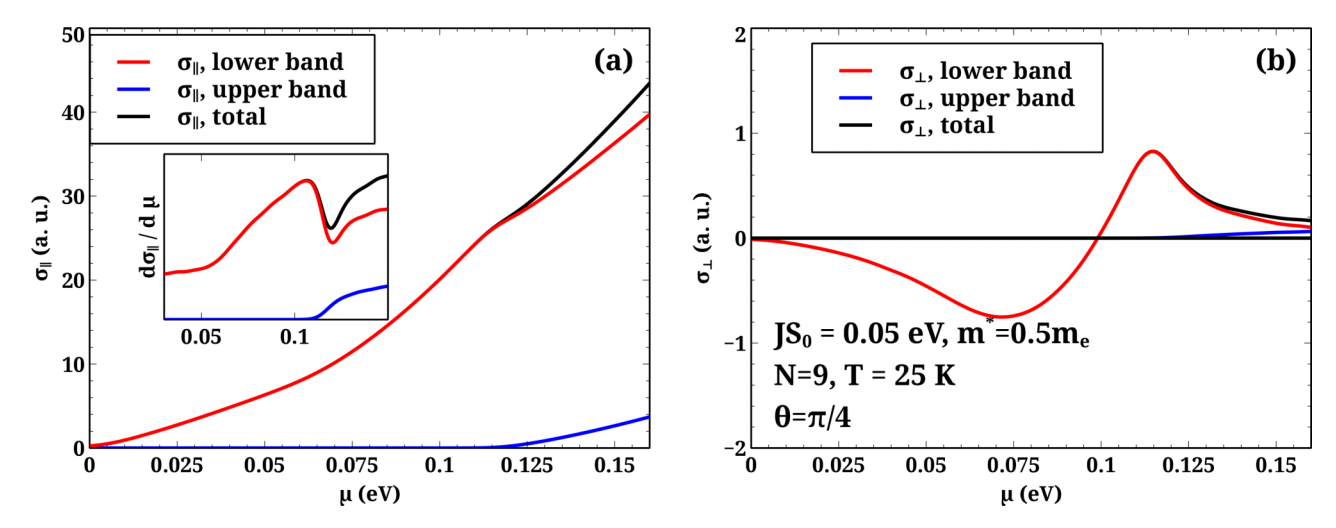


FIG. 7. (a) Direct and (b) anomalous Hall conductivities for  $\theta = \pi/4$ . The blue curves describe the conductivities for the upper band, and the red curves are for the lower band. The black lines represent the total electroconductivity. In the insertion, the derivative of the direct component of the conductivity over chemical potential is depicted.

pronounced because the bands become more anisotropic. This case also corresponds to Fig. 1(d) where the blue region is lower than for  $\theta = \pi/16$ . All the explanations of the kinks in Fig. 7(a) and maximum and minimum in Fig. 7(b) remain the same.

As mentioned above, the transition rate matrix has nonvanishing off-diagonal matrix elements. Such elements allow for the transitions between  $\varepsilon_1(\mathbf{k})$  and  $\varepsilon_2(\mathbf{k})$  bands for chemical potentials greater than the gap. In Fig. 8 we demonstrate the diagonal and nondiagonal matrix elements of  $W_{\nu\nu'}$  determined from the following Equation [16]:

$$\tau_{\nu\nu'}^{-1} = W_{\nu\nu'} = \sum_{\mathbf{k}'} W_{\nu\nu'}(\mathbf{k}, \mathbf{k}') (f_{\nu'}(\mathbf{k}') - f_{\nu}(\mathbf{k})).$$
 (25)

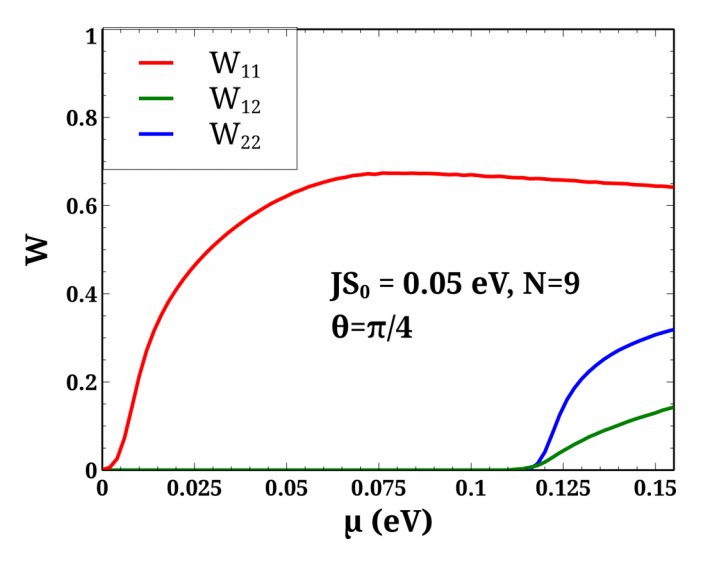


FIG. 8. Transition probability matrix elements,  $W = \tau^{-1}$ . The red curve corresponds to transitions within the lower band, the blue curve represents transitions within the upper band, and the green curve corresponds to the interband transitions.

As shown in Fig. 8, the nondiagonal matrix element (the green curve) has large values and therefore, substantially contributes to the transition between the bands, strongly affecting the electroconductivity in this region of  $\mu$ . The energy band structures for a helical state ( $\theta = \pi/2$ ) are shown in Figs. 1(b) and 1(c). The two components of the electroconductivity are presented in Fig. 9. The first kink goes to zero because of the symmetry of the bands and the absence of the maximum. However, the anomalous Hall component demonstrates the more dramatic behavior and such a dependence can be explained in the same manner as in the description of Fig. 3(b). The amplitudes are higher because the anisotropy in  $\varepsilon_1(k)$  is stronger.

# V. TEMPERATURE DEPENDENCE

The proposed theory can be verified in some experiments where phase transition from the conical (helical) to ferromagnetic (or paramagnetic) state occurs. Indeed, there is the phase transition from a helical to paramagnetic state at  $T = 28.8 \,\mathrm{K}$ in a MnSi single crystal [18]. In Fig. 10 we present the temperature dependencies for the hole resistivity of the direct and anomalous Hall components,  $\rho_{\parallel}$  and  $\rho_{\perp}$ , at the phase transition. In Fig. 10(a) the experimentally measured dependence of  $\rho_{\parallel}$  is described by the black curve, the calculated  $\rho_{\parallel}(T)$ in the helical and in the paramagnetic states are represented by the red and blue curves, respectively. Theoretical results have been scaled to numerically fit experimental data. We find the excellent agreement between the calculated results and the experimental data for the direct resistivity. In addition, in Fig. 10(b) we demonstrate the temperature dependence of  $\rho_{\perp}$ . The theory predicts the growing anomalous Hall resistivity in the helical phase and no anomalous Hall current in the paramagnetic state at  $T > T_C$ . As mentioned above, the anomalous Hall resistivity takes place only for anisotropic bands. In the absence of the helicity the bands are isotropic. Consequently, the anomalous anomalous Hall conductivity vanishes. If the spin-orbit interaction for conduction electrons is

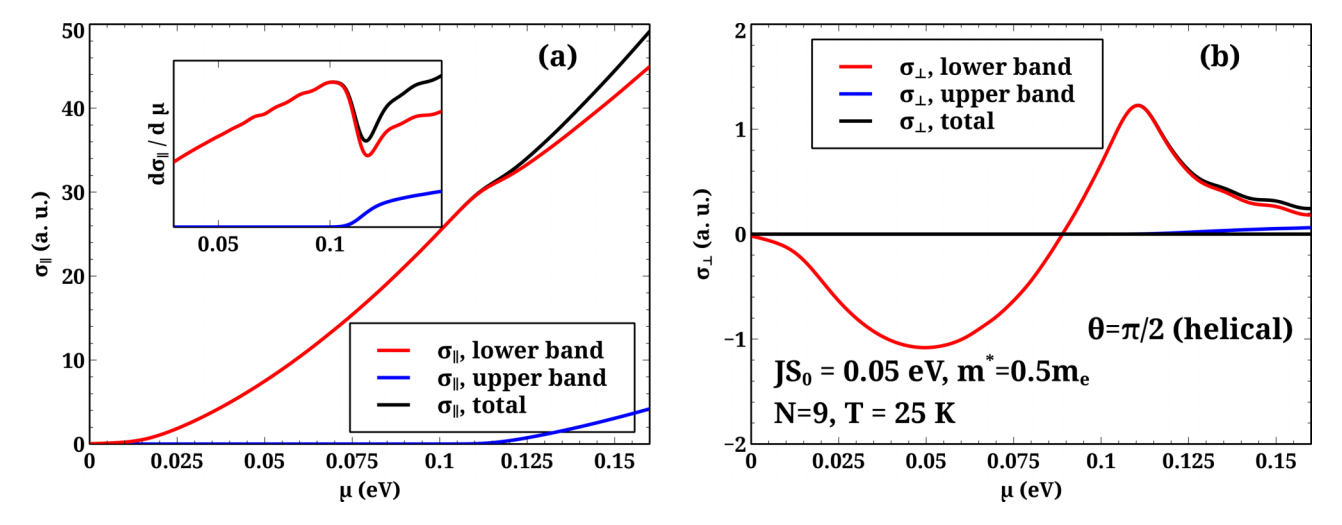


FIG. 9. (a) Direct and (b) anomalous Hall conductivities for  $\theta = \pi/2$ , the helical state. The blue curves represent the conductivities for the upper band, and the red curve is for the lower band. The black lines represent the total electroconductivity. In the insertion the derivative of the direct component of the conductivity over chemical potential is presented.

included, the anomalous Hall conductivity may go to another finite value.

The model we use for the calculations does not precisely represent MnSi. For example, it does not include many-band structure of MnSi, the bands are not shaped in such a complex way as in the real material, and the spin-orbit coupling for conduction electrons is not considered here. Nevertheless, the theory is capable to recognize and explain some of the effects observed in the experiment. Another way to investigate the particular material is to consider a realistic band structure from DFT calculations because Eqs. (7) and (8) are not restricted to parabolic energy bands. If a many-band structure is considered, the predicted effects still remain. Indeed, multiple nonparabolic bands are split in the same way as parabolic ones, and transitions due to electron-acoustic phonon scattering will still take place. More kinks similar to observed in

Figs. 4, 7, 9 may occur due to the complex shape of energy bands but the behavior of the resistivity at the phase transition should not change.

The temperature dependence of the electroconductivity stems from the two factors: (a) the equilibrium Fermi distribution function in the Boltzmann Equation (9) and (b) the Bose-Einstein distribution function in the expression for the transition probability matrix (15). In the high temperature limit, the latter yields  $W \sim T$  and therefore, conductivity  $\sigma \sim 1/T$  or resistance  $\rho \sim T$ .

### VI. BERRY CURVATURE

It is important to understand whether conical spin-spiral textures are topological structures causing the anomalous Hall effect. In order to calculate Berry curvature in a real space,

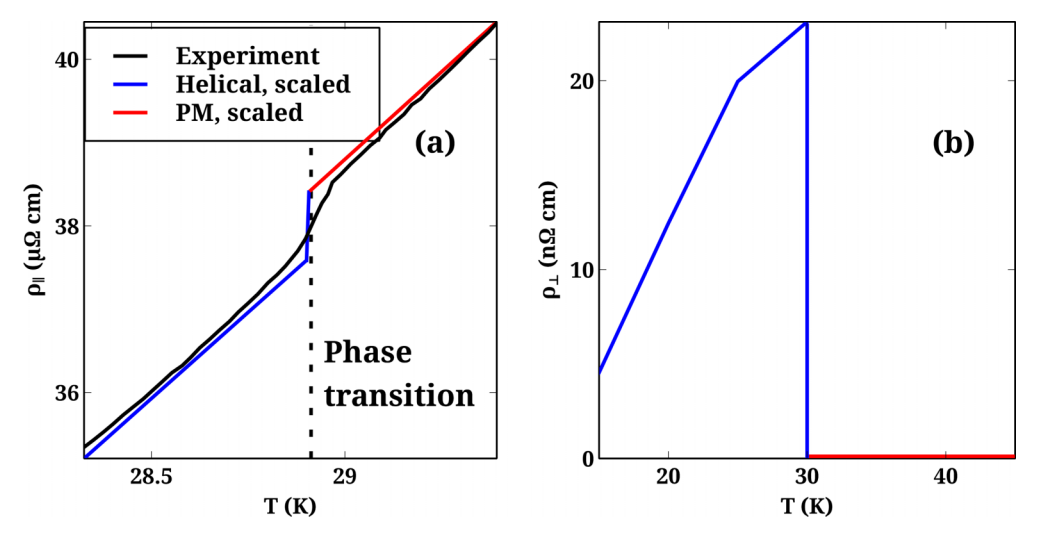


FIG. 10. Temperature dependence of the hole resistivity for a MnSi single crystal, (a) direct and (b) anomalous Hall components. The red and blue curves are theoretical and the black curve in (a) is experimental (see Ref. [18]).  $JS_0 = 0.07 \,\text{eV}$ ,  $m^* = 0.5 m_e$ ,  $n = 7.5 \times 10^{19} \,\text{cm}^{-3}$ , the period of the spiral is 36 lattice constants.

we employ the unitary transformation approach where we are looking for a unitary transformation, which diagonalizes the conical potential,

$$\hat{U}^{\dagger}(\hat{\boldsymbol{\sigma}}\cdot\boldsymbol{n})\hat{U}=\hat{\boldsymbol{\sigma}}\cdot\boldsymbol{e}_{7},\tag{26}$$

where  $\hat{U}$  is given by the following equation:

$$\hat{U} = \begin{pmatrix} \cos\frac{\theta}{2} & \sin\frac{\theta}{2}e^{-i\varphi} \\ \sin\frac{\theta}{2}e^{i\varphi} & -\cos\frac{\theta}{2} \end{pmatrix}. \tag{27}$$

Here  $\varphi(z)$  is a polar angle for the unit vector along the magnetization direction  $\mathbf{n} = (\sin \theta \cos \varphi, \sin \theta \sin \varphi, \cos \theta)$ . By

using the unitary transformation, the Hamiltonian becomes

$$\hat{U}^{\dagger}\hat{H}\hat{U} = \frac{\hat{U}^{\dagger}\boldsymbol{p}^{2}\hat{U}}{2m} - JS_{0}\sigma_{z} = \frac{(\hat{U}^{\dagger}\boldsymbol{p}\hat{U})^{2}}{2m} - JS_{0}\sigma_{z}$$

$$= \frac{(\boldsymbol{p} - i\hbar\hat{U}^{\dagger}(\boldsymbol{\nabla}\cdot\hat{U}))^{2}}{2m} - JS_{0}\sigma_{z}. \tag{28}$$

Then the product  $\hat{U}^{\dagger}\nabla\cdot\hat{U}$  can be expressed in the following way:

$$\hat{U}^{\dagger} \nabla \hat{U} = \begin{pmatrix} \frac{i}{2} (1 - \cos \theta) (\nabla \varphi) & \frac{1}{2} e^{-i\varphi} [(\nabla \theta) - i \sin \theta (\nabla \varphi)] \\ \frac{1}{2} \cos \frac{\theta}{2} e^{i\varphi} (\nabla \theta) + i \sin \frac{\theta}{2} e^{i\varphi} (\nabla \varphi) & -\frac{i}{2} (1 - \cos \theta) (\nabla \varphi) \end{pmatrix}. \tag{29}$$

We assume that the electron remains on the same energy band as it travels in r space and cannot flip between states, and use adiabatic approximation, setting off-diagonal elements of Eq. (29) to zero [21]. Using this approximation and the (1,1) diagonal matrix element in Eq. (29), we obtain the effective vector potential,

$$A^{\uparrow\uparrow} = A^{\rm ad} = \frac{\hbar}{2e} (1 - \cos\theta)(\nabla\varphi). \tag{30}$$

Because the parameters depend only on the coordinate z, the curl of the vector potential vanishes,

$$\mathbf{B}_{\text{eff}} = \frac{\hbar}{2e} \nabla \times (1 - \cos \theta) (\nabla \varphi)$$
$$= \frac{\hbar}{2e} [\nabla (1 - \cos \theta)] \times (\nabla \varphi) = 0. \tag{31}$$

Thus, we have proved that there is no effective magnetic field resulting in the absence of topological Hall effect. We also have found that the chirality change  $(\varkappa \to -\varkappa)$  does not affect electronic structure and transport properties. That was checked numerically and also can be understood from the symmetry considerations:  $\varkappa$  is included into the equations as  $(k_z \pm \varkappa/2)^2$ , and replacing  $\varkappa \to -\varkappa$  is equivalent to  $k_z \to -k_z$ . For the band structure it results in mirroring the Fig. 1, and the conductivity tensor is diagonal, so the transport properties also must stay the same.

### VII. CONCLUSIONS

In this paper we propose the theory of transport properties in conical helimagnets. The system is described by Hamiltonian (1), where the conical potential is considered in the continuum approximation. In this Hamiltonian we do not include spin-orbit coupling for conduction electrons. We should note that helimagnets can exist without Dzyaloshinskii-Moriya interaction. The helical structure can be due to the electron exchange interaction in FeP crystals as discussed in Ref. [5].

We diagonalize Hamiltonian (1) and find the energy bands  $\varepsilon_1(\mathbf{k})$  and  $\varepsilon_2(\mathbf{k})$  with corresponding eigenfunctions [see

Eqs. (7) and (8)]. For the derivations, the crystal band structure  $\varepsilon_0(\mathbf{k})$  has been chosen in the most general form.

For the lower band  $\varepsilon_1(\mathbf{k})$ , there are four different cases depending on the parameters: (a) the spherical paraboloids, (b) helical where  $\varepsilon_1(\mathbf{k})$  has one minimum, (c)  $\varepsilon_1(\mathbf{k})$  has two symmetric minima corresponding to a helical state, and (d)  $\varepsilon_1(\mathbf{k})$  is asymmetric and has one or two minima in the conical phase. We have calculated the electroconductivities for different cone half-angles  $\theta$  (see Fig. 2). We have found that in the conical state there is an anomalous Hall component in electric conductivity. However, we have proven that the Berry curvature vanishes and therefore, the nature of the anomalous Hall electroconductivity is nontopological. We have shown that the origin of the anomalous Hall current is caused by the interplay of the decrease of the momentum space in the z direction and the restrictions imposed by spin-forbidden transitions in accordance with Equation (7). We have proven that the chirality does not affect electronic structure and transport properties. To find the electroconductivites, we have used the semiclassical approach based on the Boltzmann Equation (9), which has been solved numerically. The relaxation mechanism is due to the electron-phonon interaction. For MnSi pure crystals we have proven that the optical phonons do not contribute because of the large frequency values,  $h\nu_{\rm opt} \gg k_B T_C$ . We have found that the transition rate matrix has nondiagonal matrix elements causing the interband transitions. As demonstrated in Fig. 8, the transitions between the bands are strong for higher chemical potentials. In this paper we vary only two parameters: chemical potential and temperature. The former can be changed by applying gate voltage. We have compared the proposed theory with the experiments. The theory has been verified by the comparison with the experimental temperature dependence of the direct resistivity at the helical to paramagnetic phase transition at  $T_C = 29 \,\mathrm{K}$ . As shown in Fig. 10(a), the resistivity abruptly increases at  $T = T_C$ . The excellent agreement between the theoretical calculations and the experimental data has been found. We have also predicted that the anomalous Hall resistivity has the abrupt behavior dropping to zero in the paramagnetic phase or another value if the spin-orbit coupling is not small. It could be a good

test of the theory if the anomalous Hall conductivity vanishes or have the nonzero value in the ferromagnetic phase. In the former case the proposed theory is true and in the latter one consideration of spin-orbit coupling for conduction electrons is necessary.

### ACKNOWLEDGMENTS

This work was supported by grants from the U.S. National Science Foundation (Grants No. 2228841 and No. DMR-1710512) and the U.S. Department of Energy (Grant No. DE-SC0020074) to the University of Wyoming.

- [1] J. Inoue and S. Maekawa, Phys. Rev. Lett. 74, 3407 (1995).
- [2] J. Xiao, A. Zangwill, and M. D. Stiles, Phys. Rev. B 73, 054428 (2006).
- [3] O. V. Yazyev and M. I. Katsnelson, Phys. Rev. Lett. 100, 047209 (2008).
- [4] L. D. Landau and E. M. Lifshitz, *Electrodynamics of Continuous Media* (Pergamon Press, New York, 1984).
- [5] A. S. Sukhanov, Y. V. Tymoshenko, A. A. Kulbakov, A. S. Cameron, V. Kocsis, H. C. Walker, A. Ivanov, J. T. Park, V. Pomjakushin, S. E. Nikitin, I. V. Morozov, I. O. Chernyavskii, S. Aswartham, A. U. B. Wolter, A. Yaresko, B. Büchner, and D. S. Inosov, Phys. Rev. B 105, 134424 (2022).
- [6] B. Binz and A. Vishwanath, Phys. Rev. B 74, 214408 (2006).
- [7] Y. Tsunoda, J. Phys.: Condens. Matter 1, 10427 (1989).
- [8] L. Sandratskii and J. Kübler, Phys. B: Condens. Matter 217, 167 (1996).
- [9] P. Kurz, F. Förster, L. Nordström, G. Bihlmayer, and S. Blügel, Phys. Rev. B 69, 024415 (2004).
- [10] Y. Wang, Y. Feng, J.-G. Cheng, W. Wu, J. L. Luo, and T. F. Rosenbaum, Nat. Commun. 7, 13037 (2016).
- [11] A. Zadorozhnyi and Y. Dahnovsky, Phys. Rev. B 105, 014445 (2022).

- [12] L. M. Sandratskii, Phys. Status Solidi B 136, 167 (1986).
- [13] D. Kurebayashi and N. Nagaosa, Commun. Phys. 4, 260 (2021).
- [14] P. Bruno, V. K. Dugaev, and M. Taillefumier, Phys. Rev. Lett. 93, 096806 (2004).
- [15] K. Everschor-Sitte and M. Sitte, J. Appl. Phys. 115, 172602 (2014).
- [16] A. Anselm, Introduction to Semiconductor Theory (Mir, Moscow, 1981).
- [17] D. Lamago, E. S. Clementyev, A. S. Ivanov, R. Heid, J.-M. Mignot, A. E. Petrova, and P. A. Alekseev, Phys. Rev. B 82, 144307 (2010).
- [18] S. M. Stishov, A. E. Petrova, S. Khasanov, G. K. Panova, A. A. Shikov, J. C. Lashley, D. Wu, and T. A. Lograsso, Phys. Rev. B 76, 052405 (2007).
- [19] A. Zadorozhnyi and Y. Dahnovsky, J. Phys.: Condens. Matter 35, 015701 (2023).
- [20] P. A. Alekseev, E. S. Clementyev, R. Heid, A. S. Ivanov, D. Lamago, J.-M. Mignot, A. E. Petrova, and S. M. Stishov, J. Phys.: Conf. Ser. 273, 012129 (2011).
- [21] T. Fujita, M. B. A. Jalil, S. G. Tan, and S. Murakami, J. Appl. Phys. 110, 121301 (2011).